Semaphorin7A patterns neural circuitry in the lateral line of the zebrafish

Agnik Dasgupta[1,*], Sang P. Paik[1,2], Lauren M. Snow[1,3], and A. J. Hudspeth[1,*]

[1] Howard Hughes Medical Institute and Laboratory of Sensory Neuroscience, The Rockefeller University, New York, NY, USA

*Corresponding author: Dr. Agnik Dasgupta
Laboratory of Sensory Neuroscience
The Rockefeller University
New York, NY 10065
Telephone: 212-327-7353
E-mail: adasgupta@rockefeller.edu

[2] Present address: Department of Functional Neuroanatomy, Institute for Anatomy and Cell Biology, Heidelberg University, Heidelberg, Germany

[3] Present address: Brigham and Women's Hospital, Boston, MA, USA

Abstract

In a developing nervous system, axonal arbors often undergo complex rearrangements before neural circuits attain their final innervation topology. In the lateral line sensory system of the zebrafish, developing sensory axons reorganize their terminal arborization patterns to establish precise neural microcircuits around the mechanosensory hair cells. However, a quantitative understanding of the changes in the sensory arbor morphology and the regulators behind the microcircuit assembly remain enigmatic. Here, we report that Semaphorin7A (Sema7A) acts as an important mediator of these processes. Utilizing a semi-automated three-dimensional neurite tracing methodology and computational techniques, we have quantitatively analyzed the morphology of the sensory arbors in wild-type and Sema7A loss-of-function mutants. In contrast to those of wild-type animals, the sensory axons in Sema7A mutants display aberrant arborizations with diminished contacts to hair cells. Moreover, ectopic expression of a secreted form of Sema7A by non-hair cells induces chemotropic guidance of sensory axons. Our findings demonstrate that Sema7A functions both as a juxtracrine and as a secreted cue to pattern neural circuitry during sensory organ development.

Introduction

Pathfinding axons are directed to their appropriate synaptic targets by a variety of guidance cues. While approaching or traversing the target field, the growth cones of migrating axons encounter secreted or cell surface-attached ligands and respond by steering toward or away from their sources (1–4). Fine-grained control of these factors is critical for the establishment of proper neural circuitry.

The zebrafish's lateral line provides a tractable *in vivo* system for exploring the mechanisms that guide the assembly of neural circuits in a peripheral nervous system. In particular, it is possible to detect individual hair cells and the sensory axons that innervate them throughout the first week of development (5). The primary posterior lateral line on each side of the zebrafish’s tail consists of about seven neuromasts, which contain mechanoreceptive hair cells of opposing polarities—half sensitive to headward (rostrad) water motion and the

complementary half to tailward (caudad) water motion—that cluster at their centers (6). The sensory axons of the lateral-line nerve branch, arborize, and consolidate around the basolateral surfaces of the hair cells (Fig. 1A). To aid in an animal's swimming behavior, these hair cells sense water currents and relay signals to the brain through the sensory axons (7). The well-defined structure of the ramifications and synaptic contacts of the sensory axons highlight the need to determine the molecular signals behind the assembly of such precise microcircuits (8).

We adopted a candidate-gene strategy to seek factors that direct the growth of afferent growth cones in the zebrafish's lateral line. Analysis of a single-cell RNA sequencing data identified the *semaphorin7a* (*sema7a*) gene to be highly expressed in hair cells of that organ (9). Semaphorins are important regulators of axonal growth and target finding during the patterning of diverse nervous systems (10). The semaphorin family includes proteins that are secreted, transmembrane, and cell surface-attached (11). Among these, Semaphorin7A (Sema7A) is the only molecule that is anchored to the outer leaflet of the lipid bilayer of the cell membrane by a glycosylphosphatidylinositol (GPI) linker (11). Unlike many other semaphorins, which act as repulsive cues (12,13), Sema7A is involved in promoting axon growth (4) and imparting directional signals by interacting with the integrin and plexin families of receptors residing on the pathfinding axons (14–16). Sema7A likely occurs *in vivo* in both GPI-anchored and soluble forms (17–19), and studies of neuronal explants confirm that both forms can induce directed axonal outgrowth (4). Furthermore, it has been proposed that the GPI anchor is cleaved by membrane-resident GPI-specific phospholipases (GPI-PLs) or matrix metalloproteases to release the Sema7A into the extracellular environment and thus regulate dynamic cellular processes (20,21). Because these observations indicate that Sema7A might influence neuronal development both as a juxtracrine and as a diffusive signal, we investigated the role of Sema7A in sculpting a vertebrate peripheral sensory organ.

Results

Sema7A expression and localization in hair cells. The zebrafish genome contains a single *sema7a* gene that produces two transcripts. One transcript encodes Sema7A-GPI, a full-

length, GPI-linked, cell surface-attached protein. The second transcript yields Sema7A^{sec}, a protein with a truncated C-terminus, which we conjecture is secreted into the local environment. Each transcript encodes an N-terminal signal sequence and a single copy of the conserved sema domain (11). Using primers that flank the regions encoding the sema domain and the distinct C-termini of the two transcripts, we performed reverse transcription and polymerase chain reactions (RT-PCR) to identify both the membrane-anchored and the secreted transcript in developing larvae (Fig. 1B; Fig. S1A). Single-cell RNA sequencing data also have shown that the *sema7a* transcript is particularly enriched in the immature and mature hair cells of the neuromast during early larval development (9), a period when sensory axons of the posterior lateral line contact hair cells and form synapses with them (5,22). Indeed, we have observed Sema7A to be specifically localized in both mature and immature hair cells (Fig. 1C; Fig. S1B-E).

As neuromasts mature, the contacts between sensory axons and hair cells increase in number, become stabilized, and establish synapses (5,22). Because Sema7A can modulate axon guidance (4,14) and synapse formation (15), we wondered whether the level of Sema7A also changes during neuromast development. Upon quantifying the average intensity of Sema7A, we found similar expression in rostrally and caudally polarized hair cells of neuromasts at 1.5, 2, 3, and 4 days post fertilization (dpf). The average Sema7A intensity increased significantly over this period in both rostrally and caudally polarized hair cells. At 1.5 dpf, the neuromasts harbor primarily immature hair cells that make minimal contacts with sensory axons and do not form stable association with axonal terminals (22). At this stage the average Sema7A intensity in hair cells remained low. By 2-4 dpf the hair cells mature to form stable contacts and well-defined synapses with the sensory axons (5,23). The average Sema7A intensity in hair cells at each of these stages rose to levels that significantly exceeded those of 1.5 dpf neuromasts (Fig. 1D). This rise in the amount of Sema7A during neuromast maturation supports a role for Sema7A in the guidance of sensory axons and their interaction with hair cells.

We additionally demonstrated an anisotropic distribution of Sema7A along the apicobasal axis of each hair cell. As neuromasts develop through 2, 3, and 4 dpf, Sema7A remained highly enriched in the subapical region of the hair cell, the site of the Golgi network. This localization suggests that Sema7A—like other proteins of the semaphorin family (24)—is directed to the plasmalemma through Golgi-mediated vesicular trafficking. While Sema7A maintained a high level in the subapical region, the protein increasingly accumulated at the base of the hair cell: the Sema7A level at the hair cell base was low at 2 dpf, but increased sharply by 3 dpf and 4 dpf (Fig. 1E; Fig. S1F,G). During this period the hair cells increase in number and mature, whereas the associated sensory axons arborize to contact multiple hair cells and form robust synaptic boutons at their bases (5,23). The progressive enrichment of Sema7A at the hair cell base and sensory-axon interface (Fig. 1F; Movie 1) implicates that Sema7A acts as a potential mediator of contacts between sensory axons and hair cells.

Sema7A patterns sensory axon arborizations. If Sema7A guides and restricts the sensory arbors around the hair cells clustered in a neuromast, then inactivating Sema7A function should disrupt this process. To test this hypothesis, we obtained a *sema7a* mutant allele (*sema7a*^{sa24691}) with a point mutation that introduces a premature stop codon in the conserved sema domain (Fig. S2A). The homozygous mutant, hereafter designated *sema7a*$^{-/-}$, should lack both the secreted and the membrane-attached forms of Sema7A. The average intensity of Sema7A immunolabeling in hair cells diminished by 61% in *sema7a*$^{-/-}$ larvae (0.34 ± 0.01 arbitrary units) in comparison to controls (0.87 ± 0.01 arbitrary units). In a few cases we observed minute accumulations of Sema7A at the subapical region, but little or no protein at the base of the mutant hair cells (Fig. 2A; Fig. S2B).

To characterize the impact of the *sema7a*$^{-/-}$ mutation on arbor patterning, we utilized doubly labeled transgenic fish *Tg(myo6b:actb1-EGFP;neurod1:tdTomato)* that marked the hair cells and the sensory axons of the posterior lateral line with distinct fluorophores (25). In control neuromasts, the sensory axons approached, arborized, and consolidated around the bases of clustered hair cells (Fig. 2B). Although the sensory axons approached the hair cells of *sema7a*$^{-/-}$ neuromasts, they displayed aberrant arborization patterns with wayward projections

that extended transversely to the organ (Fig. 2C). To quantitatively analyze the arborization morphology, we traced the sensory arbors in three dimensions to generate skeletonized network traces that depict–as pseudocolored trajectories–the increase in arbor length from the point of arborization (Fig. 2D,E).

To visualize the hair cell clusters and associated arborization networks from multiple neuromasts, we aligned images of hair cell clusters, registered them at their hair bundles, from neuromasts at 2 dpf, 3 dpf, and 4 dpf. Throughout development, the arborization networks of control neuromasts largely remained within the contours of the hair cell clusters; the few that reached farther nonetheless lingered nearby (Fig. 2F). This result suggests that an attractive cue retained the axons near the sensory organ. In *sema7a*$^{-/-}$ neuromasts, however the neuronal arbors failed to consolidate within the boundaries of hair cell clusters and extended far beyond them (Fig. 2G; Fig. S2C-H; Movie 2).

We quantified the distribution of the sensory arbors around the center of the combined hair cell clusters. For both the control and the *sema7a*$^{-/-}$ neuromasts, the arbor densities peaked proximal to the boundaries of the hair cell clusters. Beyond the cluster boundaries, in control neuromasts at 2 dpf, 3 dpf, and 4 dpf the arbor densities fell sharply at respectively 31.7 μm, 36.6 μm, and 32.7 μm from the center. In *sema7a*$^{-/-}$ neuromasts of the same ages, the sensory arbors extended respectively 38.5 μm, 51.4 μm, and 56.6 μm from the center (Fig. 2H; Fig. S2I-J; Fig. S5A). Furthermore, we quantified the degree of contact of the sensory arbors to their hair cell clusters in individual neuromasts from both control and *sema7a*$^{-/-}$ mutants. In control neuromasts, the degree of contact was 83 ± 1 % (mean ± SEM) at 2 dpf and 84 ± 1 % at 3 dpf, but significantly increased to 90 ± 1 % at 4 dpf (Fig. 2I; Fig. S5B). This observation indicates that the sensory arbors reinforce their association to the hair cell clusters as neuromasts develop. However, in *sema7a*$^{-/-}$ neuromasts such contact was significantly reduced. Only 69 ± 4 % of sensory arbors at 2 dpf were closely associated with the corresponding hair cell clusters, a value that remained at 67 ± 2 % at both 3 dpf and 4 dpf (Fig. 2I). These findings signify that simultaneous disruption of both signaling modalities of

Sema7A fails to restrict sensory arbors within a neuromast and significantly diminishes their contact with hair cells.

Sema7A^{sec} is a sufficient chemoattractive cue for sensory axon guidance. Because genetic inactivation of the *sema7a* gene disrupts both signaling modalities of the cognate protein, we could not assess the specific activity of the Sema7A^{sec} diffusive cue in guiding lateral-line sensory axons. To independently verify the potential role of that isoform, we therefore expressed the secreted variant ectopically and investigated the resultant arborization patterns.

Analysis of the microcircuit connectivity of the neuromasts has demonstrated bare sensory-axonal terminals in the perisynaptic compartments, where they do not contact the hair cell membrane (8). We speculate that these bare terminals are attracted by a Sema7A^{sec} diffusive cue. To test this hypothesis, we ectopically expressed Sema7A^{sec} protein tagged with the fluorophore mKate2, then analyzed its effect on the morphology of sensory arbors. Fertilized one-cell embryos were injected with the *hsp70:sema7a^{sec}-mKate2* plasmid and raised to 3 dpf. Larvae expressing the transgenesis marker—the lens-specific red fluorescent protein mCherry—were heat-shocked, incubated to allow expression, and subsequently mounted for live imaging. In these larvae, a random mosaic of cells—often embryonic muscle progenitors in the dermomyotome or mature myofibers—expressed the exogenous Sema7A^{sec}-mKate2 protein. We selected only those neuromasts in which an ectopic integration had occurred near the network of sensory arbors (Fig. 3A,B). In all 22 such cases, we observed robust axonal projections from the sensory arbor network toward the ectopically expressing Sema7A^{sec} cells. When the exogenous *sema7a^{sec}* integration occurred in embryonic muscle progenitor cells, which reside in a superficial layer external to the muscle fibers and adjacent to the larval skin (26), the projections were able to form direct contacts with them (Fig. 3C; Movies 3,4). But more often, when mature myofibers expressed the exogenous Sema7A^{sec} deep in the myotome, the axonal projections approached those targets but failed to contact them (Fig. 3D, Movies 5,6). This behavior likely arose because other components in the myotomal niche—including the fibrous epimysium, other myofibers, myoblasts, and immature

myotubes whose surroundings are permeable to diverse diffusive cues (27)—physically obstructed direct interaction of the extended neurites with the ectopically expressing myofibers. All 18 of the injected but not heat-shocked control larvae did not express ectopic Sema7A^{sec}, and we did not observe aberrant projections from the sensory arbor network (Fig. 3E).

To measure the accuracy of the extended axonal projections in finding the ectopic Sema7A^{sec} source, we defined three parameters: (1) the source path, denoted as the linear distance from the point of arborization to the boundary of an ectopically expressing Sema7A^{sec} cell; (2) the projection path, representing the linear distance from the point of arborization to the terminus of the extended projection; and (3) the projection proximity, calculated as the linear distance from the terminus of the extended axonal projection to the nearest boundary of the ectopically expressing Sema7A^{sec} cell (Fig. 3B). We quantified these parameters from 18 of the 22 mosaic integration events; in the remainder the extended axonal projections–although following the ectopic source–reentered the posterior lateral line nerve so that identification of the axon terminals was not possible (Fig. S2A-A"; Movie 7). When we plotted the projection path length against the source-path length, we observed a nearly perfect correlation (Fig. 3F). This result signifies that irrespective of the location of the ectopic source–whether proximal or distal to the sensory arbor network–the Sema7A^{sec} cue sufficed to attract axonal terminals from the sensory arbor. Furthermore, the low average projection-proximity length of 3.5 ± 0.7 μm (mean ± SEM) indicated that the extended projection terminals remained either in contact (8 of 18) or in the vicinity (10 of 18) of the ectopic Sema7A^{sec} sources (Fig. 3G). These observations together demonstrate that the Sema7A^{sec} diffusive cue is sufficient to provide neural guidance *in vivo*.

As the posterior lateral-line ganglion matures, newly formed neurons extend their axonal growth cones along the posterior lateral-line nerve to reach the neuromasts (28). We wondered whether the axonal projections that had yet to be associated with a neuromast could also respond to an ectopic source of Sema7A^{sec}. Indeed, on five occasions in which *sema7a^{sec}* integration had occurred between two neuromasts, we detected neurite extensions from the posterior lateral-line nerve to the ectopic Sema7A^{sec} source (Fig. S3B-B"; Movies 8-10). The

responsiveness of the posterior lateral line axons to Sema7A^{sec} might therefore be an intrinsic property of the neurons that does not require the neuromast microenvironment.

Effect of Sema7a deficiency on synaptic assembly. Contact stabilization between an axon and its target cell is essential for synapse formation (29). Neural GPI-anchored proteins can act as regulators of various synaptic-adhesion pathways (30). In the mouse olfactory system, GPI-anchored Sema7A is enriched in olfactory sensory axons and mediates sustained interaction with the dendrites of mitral and tufted cells in the olfactory bulb to establish synapses (15). In the developing mouse brain–particularly in Purkinje cells–GPI-anchored Sema7A instead regulates the elimination of synapses onto climbing fibers (31). The role of anchored Sema7A in regulating synaptic architecture can thus vary according to the cell type and developmental stage. Our demonstration that Sema7A is necessary to consolidate the contact between sensory axons and hair cells during neuromast development suggests a possible role in regulating synaptic structure.

Proper synaptogenesis requires the correct spatial organization of the presynaptic and postsynaptic apparatus at the apposition of two cells. At the interface between hair cells and sensory axons, the synaptic network involves two scaffolding proteins in particular: ribeye, a major constituent of the presynaptic ribbons (32), and membrane-associated guanylate kinase (MAGUK), a conserved group of proteins that organize postsynaptic densities (33). Utilizing these scaffolding proteins as markers, we investigated the impact of the *sema7a*$^{-/-}$ mutation on synapse formation. To analyze the distribution of presynaptic densities–immunolabeled with an antibody against the ribeye-associated presynaptic constituent C-terminal binding protein (CTBP) (32)–we counted the number and measured the area of CTBP punctae from multiple neuromasts at several stages of neuromast development (Fig. 4A,B). The CTBP punctae in each hair cell ranged from zero to seven across developmental stages. In the zebrafish's posterior lateral line, the formation of presynaptic ribbons is an intrinsic property of the hair cells that does not require contact with lateral-line sensory axons. However, sustained contact with the sensory axon influences the maintenance and stability of ribbons (34). As neuromasts matured from 2 dpf to 4 dpf, we identified similar distribution patterns with a characteristic

increase in the number of CTBP punctae in both control and *sema7a*$^{-/-}$ larvae (Fig. 4C,D). This result implies that the formation of new presynaptic ribbons is not perturbed in the mutants, even though there are on average fewer CTBP punctae (Fig. S4A-C). Measurement of the areas of CTBP punctae also showed similar distributions in both genotypes (Fig. 4E,F) but the average area of presynaptic densities was reduced in the mutants (Fig. S4D-F).

Because GPI-anchored Sema7A lacks a cytosolic domain, it is unlikely that Sema7A signaling directly induces formation of presynaptic ribbons. Instead, GPI-anchored Sema7A might induce postsynaptic assembly on the apposed neuronal membrane (15). To characterize the distribution of the postsynaptic aggregates–immunostained with a pan-MAGUK antibody–we performed analyses similar to those above (Fig. 4I,J). At 4 dpf, 68.3 % of the hair cells in the control neuromasts were associated with at least one MAGUK punctum. In the *sema7a*$^{-/-}$ mutant this value fell to 37.5 % (Fig. 4K,L). The average number of MAGUK punctae also declined in the mutants (Fig. S4G-I). As control neuromasts matured from 2 dpf to 4 dpf, the MAGUK punctae showed a shift toward smaller sizes, suggesting that the postsynaptic structure fragmented into smaller entities as observed in other excitatory synapses (35). At 4 dpf, 77.5 % of the hair cells in the control neuromasts had postsynaptic densities with areas between 0.10 μm^2 and 0.40 μm^2. In the *sema7a*$^{-/-}$ mutant the corresponding value was only 42.5 % (Fig. 4M,N). The average area of MAGUK punctae was also reduced in the mutants compared to the controls (Fig. S4J-L**).** We speculate that the abnormalities in postsynaptic structure arose from reduced contact between the hair cells and the sensory axons in the *sema7a*$^{-/-}$ mutants or from the lack of Sema7A-mediated juxtracrine signaling onto the apposed neurite terminals (15).

Discussion

The specification of neural circuitry requires precise control of the guidance cues that direct and restrict neural arbors at their target fields and facilitate synapse formation. In the lateral-line neuromast of the zebrafish, we have identified Sema7A as an essential cue that regulates the interaction between hair cells and sensory axons. We have discovered dual modes of

Sema7A function *in vivo*: the chemoattractive diffusible form is sufficient to guide the sensory arbors toward their target, whereas the membrane-attached form likely participates in the contact-mediated formation and maintenance of synapses. Our results suggest a potential mechanism for hair cell innervation in which a local Sema7A^{sec} diffusive cue consolidates the sensory arbors at the hair cell cluster and the membrane-anchored Sema7A-GPI molecule regulates synapse assembly.

Recent studies have begun to dissect the molecular mechanisms of semaphorin signaling in axonal navigation. In explants derived from the murine olfactory bulb, Sema7A interacts directly with integrinβ1 to trigger downstream signaling effectors involving focal adhesion kinase and mitogen-activated protein kinases, which are critical regulators of the cytoskeletal network during axonal pathfinding (4,36). Moreover, the interaction between Sema7A and its receptor plexinC1 activates the rac1-cdc42-PAK pathway, which alters the actin network to promote axonal guidance and synapse formation (15,37). We speculate that lateral-line sensory axons utilize similar mechanisms to sense and respond to Sema7A in the establishment of microcircuits with hair cells.

During early development of the posterior lateral line, the growth cones of sensory axons intimately associate with the prosensory primordium that deposits neuromasts along the lateral surface of the larva (38,39). The growth of the sensory fibers with the primordium is regulated by diverse neurotrophic factors expressed in the primordium (40,41). Impairing brain-derived or glial cell line-derived neurotrophic factors and their receptors perturbs directed axonal motility and innervation of hair cells (40,41). Lateral-line hair cells are particularly enriched in brain-derived neurotrophic factor (42) and other chemotropic cues (Fig. S6). Because the sensory axons of *sema7a*$^{-/-}$ mutants reliably branch from the lateral-line nerve to reach hair cell clusters, these chemoattractive factors might compensate in part for the absence of Sema7A function. Although sensory axons are strict selectors of hair cell polarity and form synapses accordingly (5), diverse chemoattractant cues including Sema7A occur uniformly between hair cell polarities (42). It seems likely that unbiased attractive signals bring sensory arbors toward hair cells, after which polarity-specific molecules on hair cell surfaces dictate the final

association between axonal terminal and hair cells. Notch-delta signaling and its downstream effectors regulate hair cell polarity and the innervation pattern (6,8,25). It would be interesting to determine whether Notch-mediated polarity signatures on the hair cell's surface can refine the neuromast neural circuitry.

Materials and Methods

Zebrafish strains and husbandry. Experiments were performed on 1.5-4 dpf zebrafish larvae in accordance with the standards of Rockefeller University's Institutional Animal Care and Use Committee. Naturally spawned and fertilized eggs were collected, cleaned, staged, and maintained at 28.5 ºC in system-water with 1 µg/mL methylene blue. Wild-type AB and heterozygous mutant *semaphorin7a*^{sa24691} zebrafish were obtained from the Zebrafish International Resource Center. In addition, the following transgenic zebrafish lines were used: *Tg(myo6b:actb1-EGFP)* (43), *Tg(neurod1:tdTomato)* (25), and *TgBAC(neurod1:EGFP)* (44).

Genotyping of mutant fish. The *semaphorin7a*^{sa24691} allele harbors an A-to-T point mutation in the seventh exon of the *semaphorin7a* gene, which creates a premature stop codon (Fig. S2A). Genomic DNA was isolated from the tail fins of adult *semaphorin7a*^{sa24691} (*sema7a*^{sa91}) heterozygous mutant zebrafish. The mutant locus in the genome was PCR amplified using the following primers: sema7a^{sa91}F: 5´-AAAGCTGGAAAGCGAATCAA-3´ and sema7a^{sa91}R: 5´-ATATCCAAGGATCCGCCTCT-3´. The 734-base pair amplicons were sequenced, and heterozygous adults were propagated.

Reverse transcription-polymerase chain reactions (RT PCR). Total RNA was isolated from whole zebrafish larvae by TRIzol extraction followed by DNAse treatment (TURBO DNA-free Ambion). We used thirty 4 dpf zebrafish larvae to isolate total RNA. We generated cDNA libraries using iScript cDNA Synthesis Kit (Bio-Rad). Each transcript was PCR amplified using the following primers: sema7aF: 5´-GGTTTTTCTGAGGCCATTCC-3´, sema7aR1: 5´-GGCACTCGTGACAAATGCTA-3´, sema7aR2: 5´-TGTGGAGAAAGTCACAAAGCA-3´ (Fig. S1A).

Transient transgenesis with the hsp70l:sema7a^{sec}-mKate2 construct. The pDNR-LIB plasmid containing the *sema7a^{sec}* coding sequence was purchased from horizon (7140389, Perkin-Elmer). The coding sequence was PCR amplified using the following primers: sema7a^{sec}F: 5´-GGGGACAAGTTTGTACAAAAAAGCAGGCTTGATGATTCGACATTATTCT-3´ and sema7a^{sec}R: 5´-GGGGACCACTTTGTACAAGAAAGCTGGGTG*CTT*TGTGGAGAAAGTCACAAAGCA-3´. The italicized nucleotides denote the mutated stop codon. The amplicon was then cloned into the pDONR221 vector by BP recombination to generate the middle entry pME-sema7a^{sec} vector. To generate the hsp70:sema7a^{sec}-mKate2 construct, gateway cloning was performed by combining the plasmids p5E-hsp70 (45), pME-sema7a^{sec}, p3E-mKate2-myc no-pA (Addgene, 80812), and pDESTtol2pACrymCherry (Addgene, 64023) with LR Clonase II Plus (Invitrogen). Verified constructs (25 ng/µl plasmid DNA) were injected with Tol2 Transposase mRNA (approximately 25 ng/µl) into one-cell embryos. The transiently transgenic larvae—identified by the expression of red fluorescent protein (mCherry) in their lenses—were raised till 3 dpf, heat-shocked in a water bath at 37 ºC for 1 hr, incubated at 28 ºC for 1 hr to allow expression, and subsequently mounted for live imaging.

Microscopy and volumetric rendering of living neuronal arbors and cells. Living larvae were dechorionated, anaesthetized in 600 µM 3-aminobenzoic acid ethyl ester methanesulfonate in system-water with 1 µg/mL methylene blue, and mounted in 1 % low-melting-point agarose on a glass-bottom MetTek dish at specific stages. The larvae were maintained at 28 °C during imaging in a temperature-controlled stage top chamber (OKO Lab UNO-T). Images at successive focal depths were captured at 200 nm intervals and deconvolved with Microvolution software in ImageJ (NIH). The three-dimensional datasets were processed and volume-rendered with the surface evolver and filament-tracer tools in Imaris (Bitplane, Belfast, UK). The Imaris workstation was provided by the Rockefeller University Bio-imaging Resource Center.

Immunofluorescence microscopy. For the immunofluorescence labeling of wholemounted wild-type control and *sema7a*$^{-/-}$ larvae, 1.5-4 dpf larvae were fixed overnight at 4 °C in 4 % formaldehyde in phosphate-buffered saline solution (PBS) with 1 % Tween-20 (1 % PBST). Larvae were washed four times with 1 % PBST for 15 min each, then placed for 2 hr in blocking solution containing PBS, 2 % normal donkey serum (NDS), 0.5 % Tween-20, and 1 % BSA. Primary antibodies were diluted in fresh blocking solution and incubated with the specimens overnight at 4 °C. The primary antibodies were goat anti-Sema7A (1:200; AF1835, R&D Systems) (14), rabbit anti-myosin VI (1:200; Proteus 25-6791), murine anti-GM130 (1:200; 610822, BD Transduction Laboratories), murine anti-CTBP (1:200; B-3, SC-55502, Santa Cruz Biotech), and rabbit anti-mCherry (1:200; GTX128508, GeneTex). Larvae were washed four times with 0.1% PBST for 15 min each. Alexa Fluor-conjugated secondary antibodies (Invitrogen, Molecular Probes) applied overnight at 1:200 dilutions in 0.2 % PBST included anti-rabbit (488 nm), anti-goat (555 nm), and anti-mouse (647 nm). Larvae were then washed four times in 0.2 % PBST for 15 min each and stored at 4 °C in VectaShield (Vector Laboratories).

For the immunofluorescence labeling of postsynaptic density in wholemounted wild-type control and *sema7a*$^{-/-}$ larvae, 2-4 dpf larvae were fixed with 4 % formaldehyde in PBS for 4.5-6 hr at 4 °C. Larvae were washed five times with 0.01 % PBST for 5 min each and then rinsed in distilled water for 5 min. The larvae were permeabilized with ice-cold acetone at -20 °C for 5 min. They were rinsed in distilled water for 5 min, washed five times with 0.01 % PBST for 5 min each, and blocked overnight with PBS buffer containing 2 % goat serum and 1 % BSA. Murine anti-pan-MAGUK antibody (1:500; IgG1 NeuroMab, K28.86, 75-029) was diluted in PBS containing 1 % BSA, added to the larvae, and incubated for 3 hr at room temperature. Larvae were washed five times for 5 min each with 0.01 % PBST. Alexa Fluor 555-conjugated anti-mouse secondary antibody (1:1000) diluted in PBS containing 1 % BSA was added to the larvae and incubated for 2 hr at room temperature. Larvae were washed five times with 0.01 % PBST for 5 min each, rinsed in distilled water for 5 min, and stored at 4 °C in VectaShield (Vector Laboratories).

Posterior segments of fixed larvae were mounted on a glass slide and imaged with a microlens-based, super-resolution confocal microscope (VT-iSIM, VisiTech international) under 60X and 100X, silicone-oil objective lenses of numerical apertures 1.30 and 1.35, respectively. Images at successive focal depths were captured at 200 nm intervals and deconvolved with the Microvolution software in ImageJ.

Measurement of Sema7A intensity. The average Sema7A fluorescence intensities of the hair cells from 1.5 dpf, 2 dpf, 3 dpf, and 4 dpf neuromasts were measured by determining the mean gray level within each hair cell labeled by actin-GFP expression. The intensity distribution of Sema7A protein along the apicobasal axis of the hair cell was measured using the line profile tool in ImageJ (Fig. S1F). Because hair cell lengths differed among samples, lines were drawn with 2 µm widths and varying lengths of 6-8 µm. For each hair cell, apicobasal length was scaled from 0 to 100 arbitrary units and the intensity values from 0 to 1 arbitrary units.

Generation of skeletonized networks. The labeled sensory axons were traced in three dimensions with ImageJ's semi-automated framework, SNT (46). Each trace depicts the skeletonized form of the posterior lateral-line nerve, the posterior lateral-line branch, and the point of arborization from which the sensory arbors radiate to contact the hair cells (Fig. 2D,E). The three-dimensional pixels or voxels obtained from the skeletonized sensory arbor traces were processed using custom code written in Python for visual representation and quantitative analysis.

Generation of combined hair cell clusters and the corresponding combined skeletonized networks. The hair cell clusters of neuromasts from each developmental stage were aligned by the centers of their apices, which were identified by the hair bundles, and overlayed to generate combined hair cell clusters using custom Python code. The associated skeletonized sensory-arbor traces at each developmental stage were aligned similarly using custom Python code. The details of the procedures are available upon request and the corresponding code is available on GitHub.

Quantification of sensory arbor distributions around hair cell clusters. The region from the center of the combined hair cell cluster to 60 µm in the post-cluster region was divided into 3600 concentric sections of equal area (Fig. S5A). Each section, as depicted with a distinct color shade, had an area of π µm^2. Sensory arbor density was defined as Log_{10}[(Area occupied by the arbors in each section)/ (Area of each section)]. The arbor density was then plotted as a histogram against distance from the center of the combined hair cell cluster. Each bin of the histogram represents an area of π μm^2. The histograms were finally represented as density trace graphs with Kernel Density Estimation (KDE) in Python.

Quantification of contact between sensory arbors and hair cell clusters. For each hair cell cluster, the voxels of the sensory arbor traces that were inside or within 0.5 μm—the average neurite radius—of the cluster boundary were denoted as arbors in contact with their corresponding hair cell cluster (Fig. S5B). The percentage of arbors in contact with each hair cell cluster was defined as: (Number of voxels that remained inside the cluster boundary/Total number of voxels in the arbor)X100. The data were analyzed through an automated pipeline with custom code.

Quantification of aberrant sensory arborization in ectopic Sema7A^{sec} expression. The sensory arbor networks were traced in three dimensions with SNT. The surface of each of the ectopically expressing Sema7A^{sec}-mKate2 cells was represented by a single point that was closest to the terminal point of the guided neurite. Distances between two points were calculated using standard mathematical operations.

Statistical analysis. Data visualization and statistical analysis were conducted with GraphPad Prism (Version 9). The Mann-Whitney test was used for hypothesis testing, and the statistical details are given in the respective figure legends.

Data and code availability. Owing to size restrictions, the experimental image data have not been uploaded to a repository but are available from the corresponding author on request. The

code generated during this study is available on GitHub (https://github.com/agnikdasgupta/Sema7A_regulates_neural_circuitry).

Acknowledgments. The authors thank Adrian Jacobo, Caleb Reagor, and Nicolas Velez for valuable discussions and data processing. Samantha Campbell and Anna Kaczynska provided expert fish husbandry. Katie Kindt kindly provided various strains of zebrafish. Image processing benefitted from facilities at the Bio-Imaging Resource Center. A.D. was supported by a Kavli Neural Systems Institute Postdoctoral Fellowship from Rockefeller University. S.P.P. and L.M.S. were supported by Howard Hughes Medical Institute, of which A.J.H. is an Investigator.

Author Contributions

A.D. initiated the project, conducted experiments, and quantified results. S.P.P. developed the Python codes for image analysis and quantified results. L.M.S. conducted preliminary experiments. A.D. wrote the paper with contributions from A.J.H.

Declaration of Interests

The authors declare no competing interests.

Figure Legends

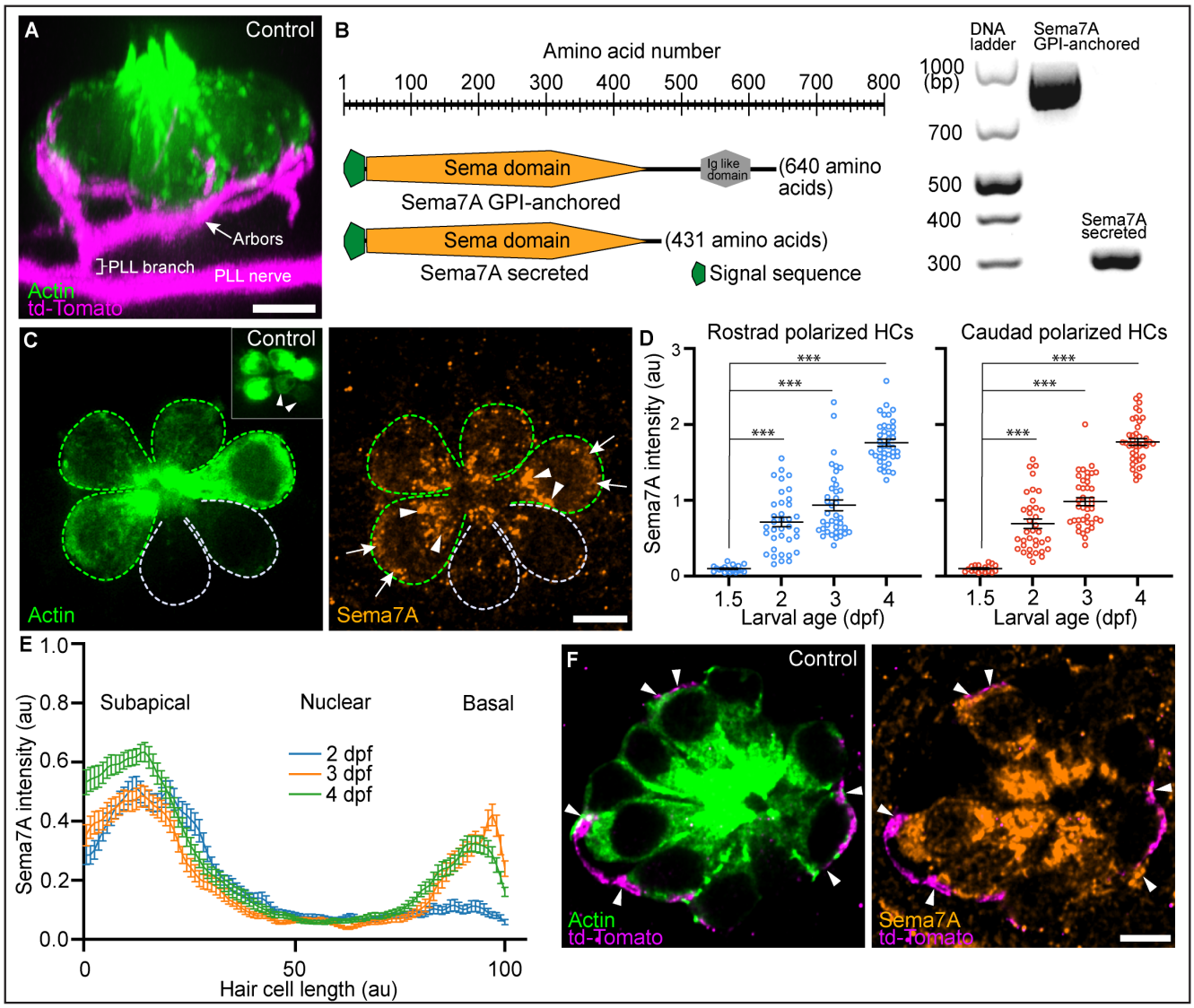

Figure 1. Expression of Semaphorin7A in the zebrafish's lateral line. (A) A volumetric rendering of a PLL neuromast depicts the sensory axons (magenta) that branch from the lateral line nerve to arborize around the basolateral surface of the hair cell cluster (green). Additional cell types in the neuromast are not labeled. Larval age, 3 dpf. (B) A schematic drawing of the two variants of the Sema7A protein molecule depicts the full-length GPI-anchored form and the smaller, potentially secreted form. Both the molecules include a signal sequence (green) and a conserved sema domain (orange). Gel-based RT-PCR analysis indicates the presence of

both the variants in developing larva. (C) A surface micrograph of a neuromast at 3 dpf depicts two pairs of mature hair cells (green dashed lines) and a pair of immature hair cells (grey dashed lines). Inset: among the three pairs of hair cell apices, the immature pair is indicated by arrowheads. Immunolabeling reveals that the Sema7A protein (orange) occurs consistently at the subapical region (arrowheads) and at the basolateral surface (arrows) of a hair cell. In this and in each of the subsequent neuromast images, anterior is to the left and ventral to the top. (D) A plot quantifies developmental changes in the average Sema7A intensity in both rostrally and caudally polarized hair cells of neuromasts from 1.5 dpf to 4 dpf. The data stem from 18, 36, 39, and 40 hair cells in neuromasts of respectively 1.5 dpf, 2 dpf, 3 dpf, and 4 dpf larvae. (E) A plot quantifies the distribution of average Sema7A intensity along the hair cell's apicobasal axis. The results stem from 52, 57, and 54 hair cells of neuromasts from 2 dpf, 3 dpf, and 4 dpf larvae. (F) An immunofluorescence image at the nuclear level of a 4 dpf neuromast shows the contact of the sensory arbors (magenta) with the basolateral surface of the hair cells (green). Immunolabeling for Sema7A (orange) reveals enrichment of the protein at the hair cell bases and sensory-axon interfaces (arrowheads). HC, hair cell; Scale bars, 5 μm; au, arbitrary unit; means ± SEMs; *** implies $p < 0.001$.

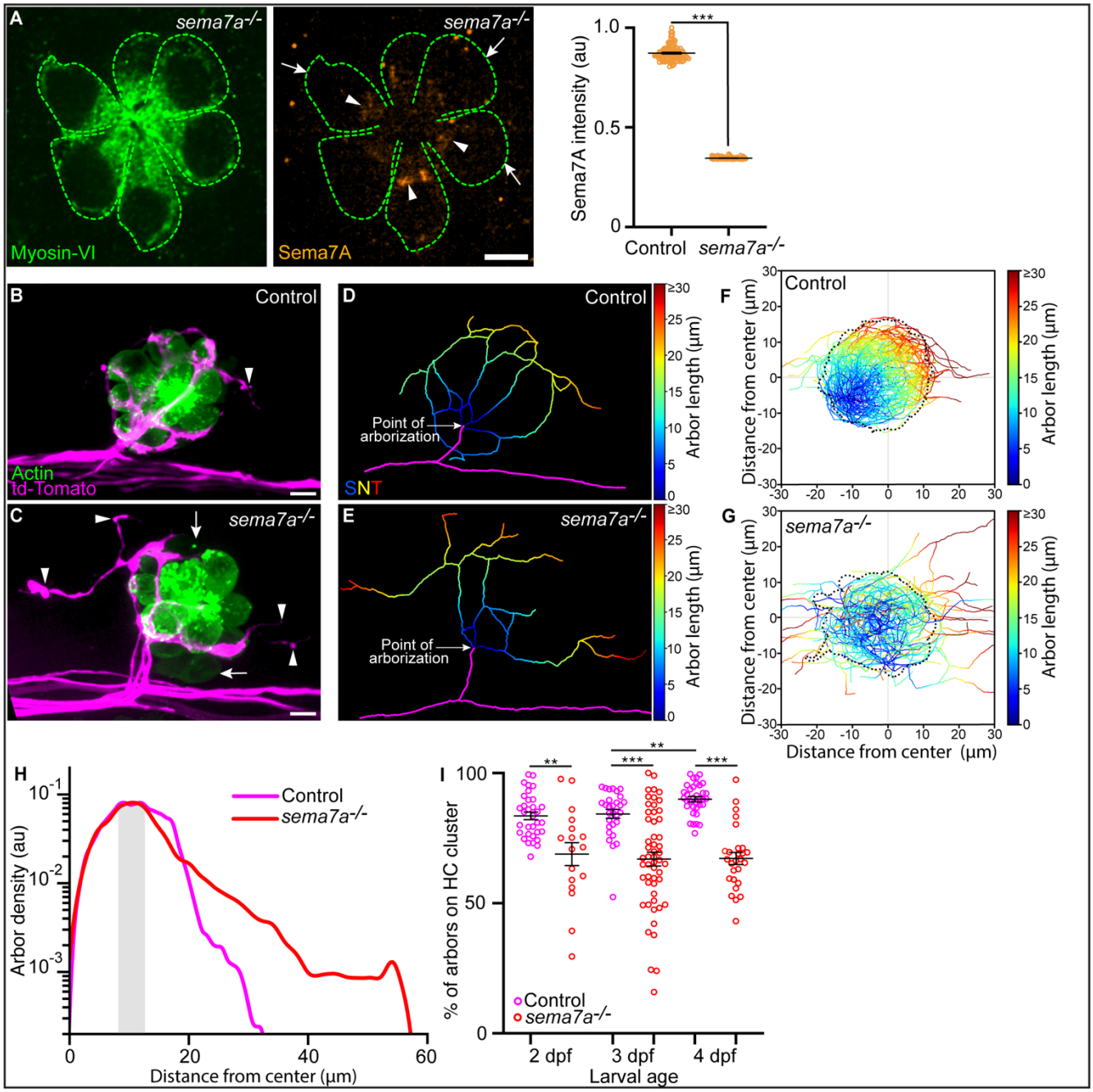

465 **Figure 2. *sema7a*$^{-/-}$ mutants display aberrant sensory axon arborizations.** (A) In a
466 micrograph of a 3 dpf *sema7a*$^{-/-}$ neuromast, Myosin VI (green) marks the hair cells (green
467 dashed lines) in which the level of Sema7A (orange) is highly reduced, with sporadic
468 localization in the subapical region (arrowheads) and none in the basolateral (arrow) region. A
469 plot of normalized Sema7A intensity from 99 control and 100 *sema7a*$^{-/-}$ hair cells quantitates

the effect. (B,C) Surface views of a control and a *sema7a*$^{-/-}$ neuromast at 4 dpf depict the interaction of the sensory arbors (magenta) with hair cell clusters (green). In the control, the arbors intimately contact the hair cells, with a few exceptions (arrowhead). In the *sema7a*$^{-/-}$ mutant, the arbors direct many aberrant projections (arrowheads) away from the hair cell cluster. The two immature hair cell pairs in the *sema7a*$^{-/-}$ neuromast are indicated by arrows. (D,E) Skeletonized networks portray the three-dimensional topology of the sensory arbors from the control and the *sema7a*$^{-/-}$ neuromasts depicted in panels B and C. The pseudocolored trajectories depict the increase in arbor contour length from each point of arborization, defined as the point at which the lateral line branch (magenta) contacts hair cell cluster. (F,G) Micrographs depict the skeletonized networks of the combined 4 dpf hair cell clusters, whose centers are located at (0,0). The X- and Y-coordinates represent the anteroposterior (AP) and the dorsoventral (DV) axes of the larva, respectively. Positive values of the X- and Y-coordinates represent the posterior and ventral directions, respectively. Combined skeletonized network traces from 27 control and 27 *sema7a*$^{-/-}$ mutant neuromasts are represented. H) The plot denotes the densities of the sensory arbors around the center of the combined hair cell clusters for 35 control (magenta) and 27 *sema7a*$^{-/-}$ (red) neuromasts at 4 dpf. The shaded area marks the region proximal to the boundary of the combined hair cell cluster. (I) The plot quantifies the degree of contact of the sensory arbors to their hair cell clusters in individual neuromasts from both control (magenta) and *sema7a*$^{-/-}$ mutants (red), each point represents a single neuromast. Thirty-three, 29, and 35 neuromasts were analyzed from 2 dpf, 3 dpf, and 4 dpf control larvae, respectively. Seventeen, 53, and 27 neuromasts were analyzed from 2 dpf, 3 dpf, and 4 dpf *sema7a*$^{-/-}$ mutant larvae, respectively. HC, hair cell; Scale bars, 5 μm; au, arbitrary unit; means ± SEMs; *** implies $p < 0.001$; ** signifies $p < 0.01$.

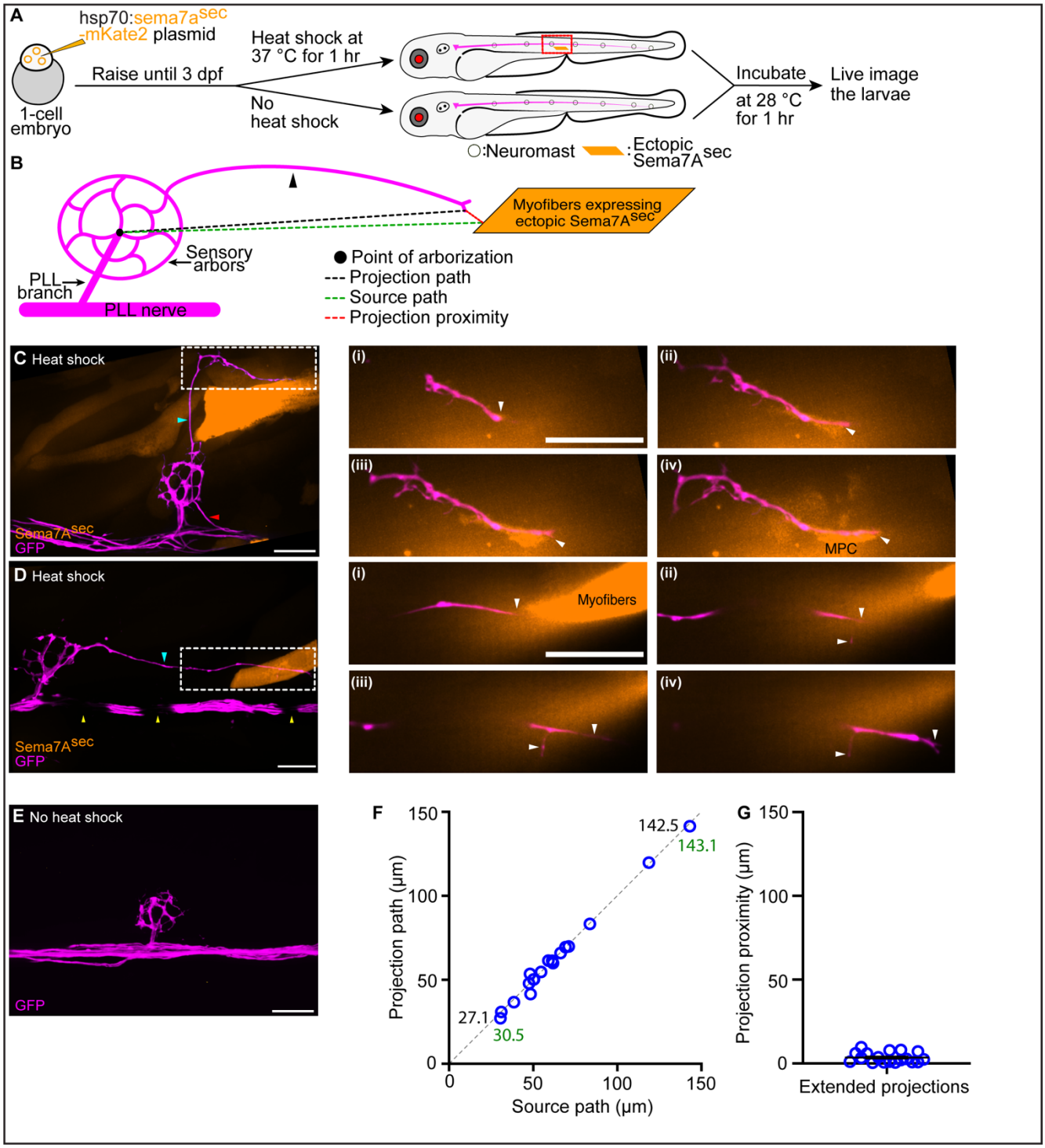

494 **Figure 3. Ectopic Sema7A^{sec} diffusive cue provides neural guidance *in vivo*.** (A) A
495 diagrammatic overview depicts the generation of a transgenic animal that expresses the
496 Sema7A^{sec} protein ectopically under the control of a thermally inducible promoter. Larvae with

ectopic myotomal-integration near the network of sensory arbors (red line) were imaged to analyze arbor morphology. (B) A schematic drawing of a sensory arbor from a heat-shocked larva depicts an extended axonal projection (arrowhead) that reaches toward the myofibers expressing the ectopic Sema7A^{sec} protein. Parameters that quantitate the accuracy of the extended axonal projections toward the ectopic Sema7A^{sec} sources are denoted. (C) In a micrograph of an ectopically expressing Sema7A^{sec} (orange) larva, the sensory arbor (magenta) extends two aberrant axonal projections. One elongates (cyan arrowhead) along the somite boundary to reach and contact an ectopically integrated muscle progenitor cell (white dashed line) and the other (red arrowhead) reenters the posterior lateral line nerve while following a second ectopic source. The through-focus scan (i–iv) from the epidermis to the dermomyotome reveals the intimate contact between the aberrant sensory arbor (arrowheads) and the muscle progenitor cell. MPC, muscle progenitor cell. (D) In a micrograph of an ectopically expressing Sema7A^{sec} (orange) larva, the sensory arbor (magenta) extends a single aberrant axonal process (cyan arrowhead) to reach ectopically integrated myofibers (white dashed line). The through-focus scan (i–iv) from the epidermis to the deep myotome reveals the proximal association of the aberrant sensory arbor (arrowheads) to the myofibers. Melanocytes (yellow arrowhead) along the horizontal myoseptum intermittently block the visibility of the lateral line nerve. (E) An injected, but not heat-shocked, control larva does not express ectopic Sema7A^{sec} and does not show aberrant projection from the sensory arbor. (F) A plot demonstrates the accuracy of 18 extended axonal arbors in finding ectopic Sema7A^{sec} sources. Each circle represents a single ectopic integration event. The two pairs of numbers represent the minimal and maximal lengths of the projection path (black) and its corresponding source path (green). (G) A plot quantitates the distribution of projection-proximity length from 18 ectopic integration events. Scale bars, 20 μm; means ± SEMs.

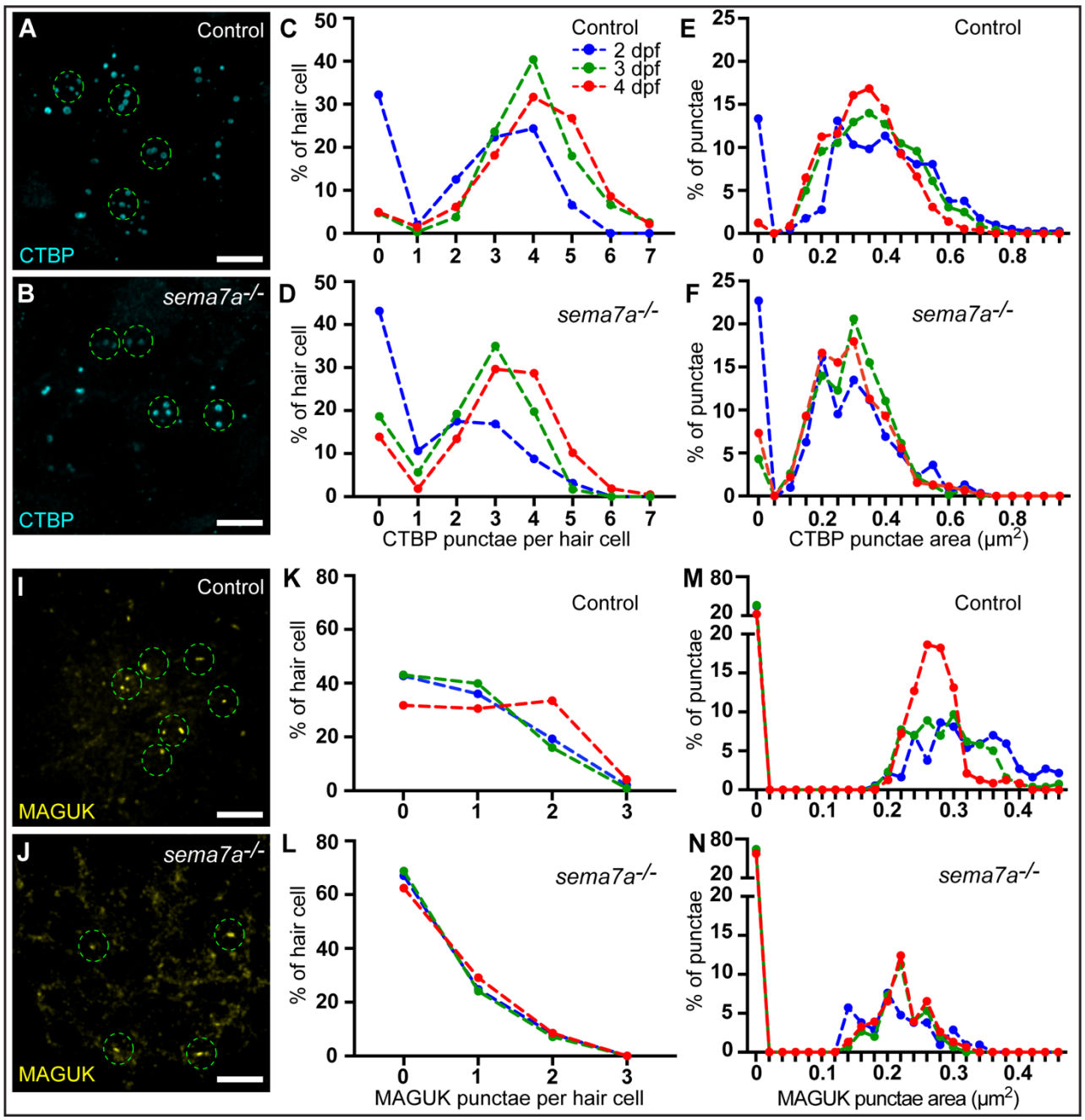

Figure 4. Sema7a deficiency impairs synaptic assembly. (A,B) Maximal-intensity projections of micrographs from a control and a *sema7a*$^{-/-}$ neuromast depict the presynaptic aggregates marked by CTBP (cyan). The approximate hair cell basal region is outlined by dashed green circles. (C-F) Plots quantitate the numbers of presynaptic aggregates (C,D) and their areas (E,F), in each hair cell across developmental stages. One hundred and fifty-two,

317, and 325 hair cells were analyzed from 2 dpf, 3 dpf, and 4 dpf control larvae, respectively. One hundred and sixty, 216, and 177 hair cells were analyzed from 2 dpf, 3 dpf, and 4 dpf *sema7a*$^{-/-}$ mutant larvae, respectively. (I,J) Maximal-intensity projections from micrographs of a control and a *sema7a*$^{-/-}$ neuromast depict the postsynaptic aggregates marked by MAGUK (yellow). The approximate hair cell basal region is outlined by dashed green circles. (K,N) Plots quantitate the numbers of postsynaptic aggregate (K,L) and their areas (M,N), in each hair cell across developmental stages. One hundred and fifty, 218, and 167 hair cells were analyzed from 2 dpf, 3 dpf, and 4 dpf control larvae, respectively. Ninety-seven, 141, and 141 hair cells were analyzed from 2 dpf, 3 dpf, and 4 dpf *sema7a*$^{-/-}$ mutant larvae, respectively. Scale bars, 5 μm.

538 **Supplementary Figure Legends**

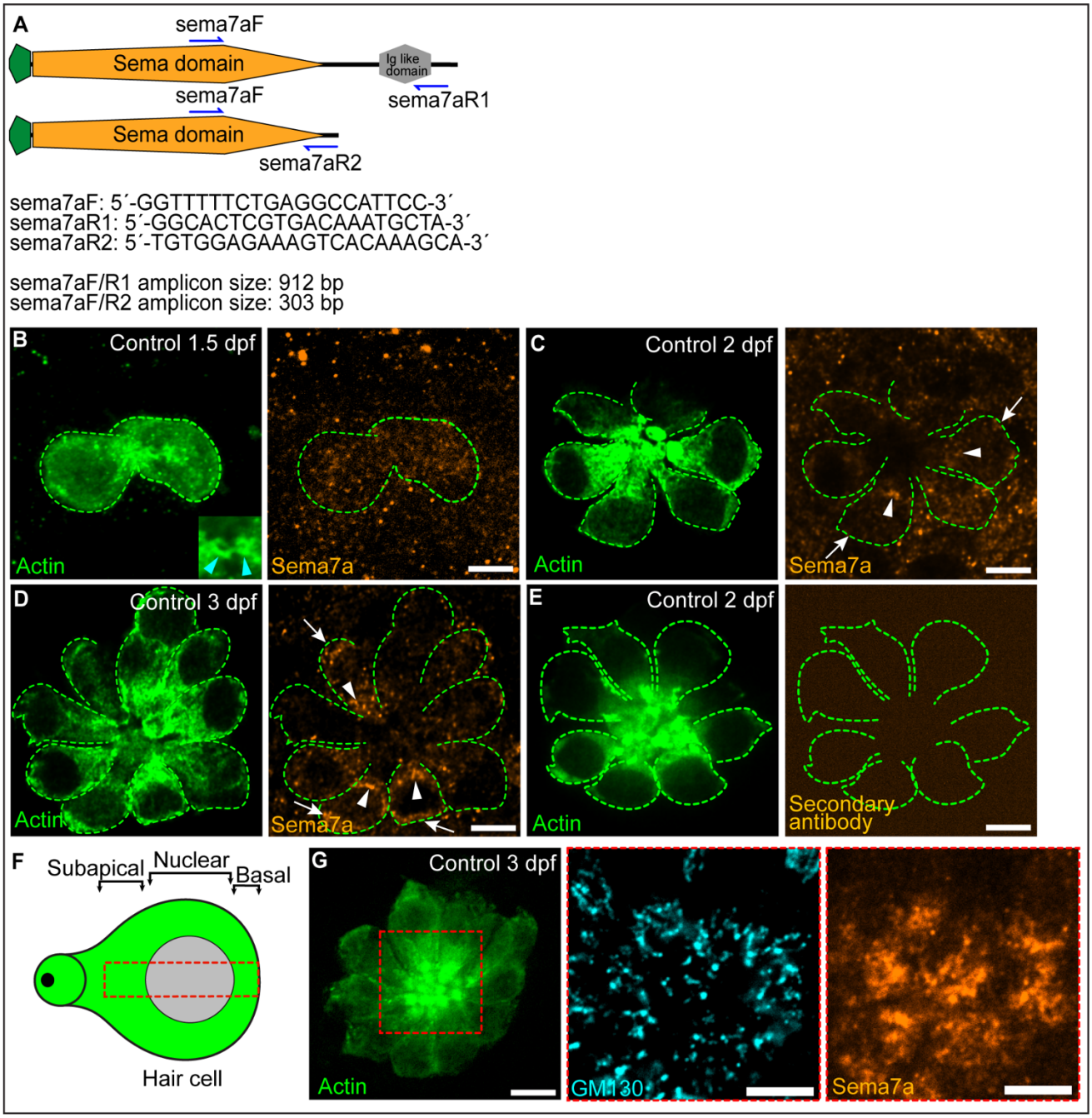

539 **Supplementary Figure 1. Expression of Semaphorin7A in the lateral line neuromast.**
540 (A) Distinct sets of primers (arrows) identify the two variants of the Sema7A protein molecule.
541 (B-D) Surface micrographs show hair cells marked with actin-GFP (green dashed lines) and
542 the localization of Sema7A protein (orange) in the subapical (arrowheads) and basal regions

(arrows) of the corresponding hair cells from neuromasts of developing control larvae. The inset in panel B depicts the apices of the immature hair cell pair. (E) Immunolabeling with only the secondary antibody fails to detect any Sema7A signal. (F) A schematic diagram of a single hair cell depicts the three distinct regions along the apicobasal axis of the cell. Sema7A intensity was measured along this apicobasal axis (red dashed line). (G). A surface micrograph depicts hair cells (green, left) whose subapical region (red dashed line) harbors the Golgi network (cyan, middle) where the Sema7A protein is enriched (orange, right). Scale bars, 5 μm.

Supplementary Movie 1. Sema7A is enriched at the hair cell base and sensory-axon interface. A through-focus scan of a 4 dpf control neuromast depicts the hair cells (green) that are innervated by the sensory axons (magenta) at their basolateral surfaces where the Sema7A protein (orange) is highly enriched. Scale bar, 5 μm.

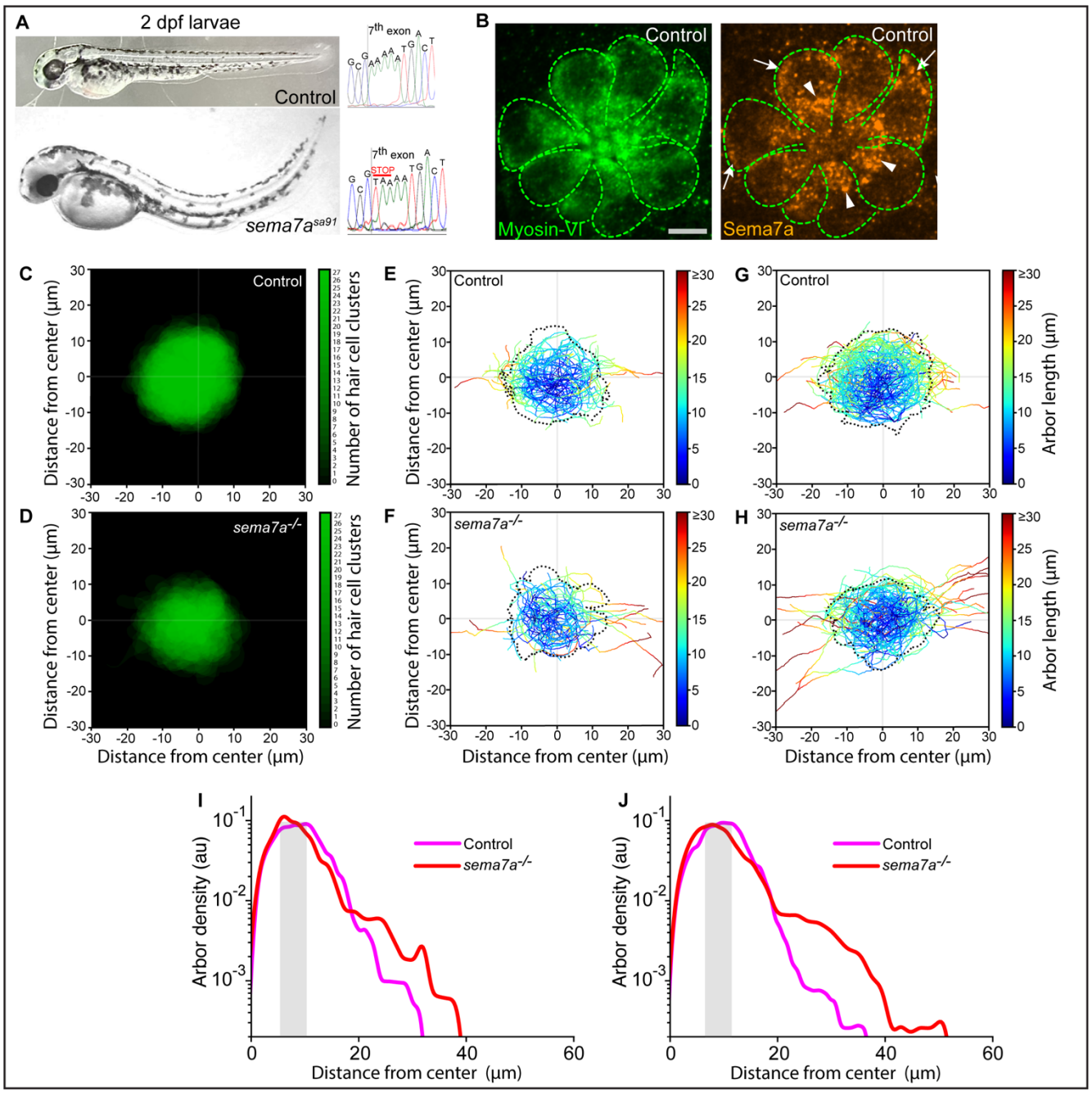

Supplementary Figure 2. *sema7a*$^{-/-}$ mutants exhibit aberrant sensory-axon arborization throughout development. (A) Micrographs depict the overall morphologies and *sema7a* genomic profiles of 2 dpf control (top) and *sema7a*$^{-/-}$ larvae (bottom). (B) In a surface micrograph of a 3 dpf control neuromast, myosin VI (green) marks hair cells (green dashed lines). Sema7A (orange) protein is highly enriched in the subapical region (arrowheads) and basolateral (arrow) region of the hair cells. (C,D) Micrographs depict combined 4 dpf hair cell clusters, each of whose centers arise located at (0,0). The X- and Y-coordinates represent the anteroposterior (AP) and dorsoventral (DV) axes of the larva, respectively. Positive values of

the X- and Y-coordinates represent posterior and ventral directions, respectively. Combined hair cell clusters from 27 control and 27 *sema7a*$^{-/-}$ mutant neuromasts are represented. (E,F) Micrographs depict the skeletonized networks of the combined 2 dpf hair cell clusters from 17 control and 17 *sema7a*$^{-/-}$ mutant neuromasts. (G,H) Micrographs depict the skeletonized networks of the combined 3 dpf hair cell clusters from 29 control and 29 *sema7a*$^{-/-}$ mutant neuromasts. (I) A plot quantitates the densities of the sensory arbors around the center of the combined hair cell clusters for 33 control (magenta) and 17 *sema7a*$^{-/-}$ (red) neuromasts at 2 dpf. The shaded area marks the region proximal to the boundary of the combined hair cell cluster. (J) A plot quantitates the densities of the sensory arbors around the center of the combined hair cell clusters for 29 control (magenta) and 53 *sema7a*$^{-/-}$ (red) neuromasts at 3 dpf. The shaded area marks the region proximal to the boundary of the combined hair cell cluster. Scale bar, 5 μm; au, arbitrary units.

Supplementary Movie 2. Three-dimensional arborization patterns in control and *sema7a*$^{-/-}$ neuromasts. Lateral views depict three-dimensionally rendered combined skeletonized network traces from 27 control and 27 *sema7a*$^{-/-}$ mutant neuromasts.

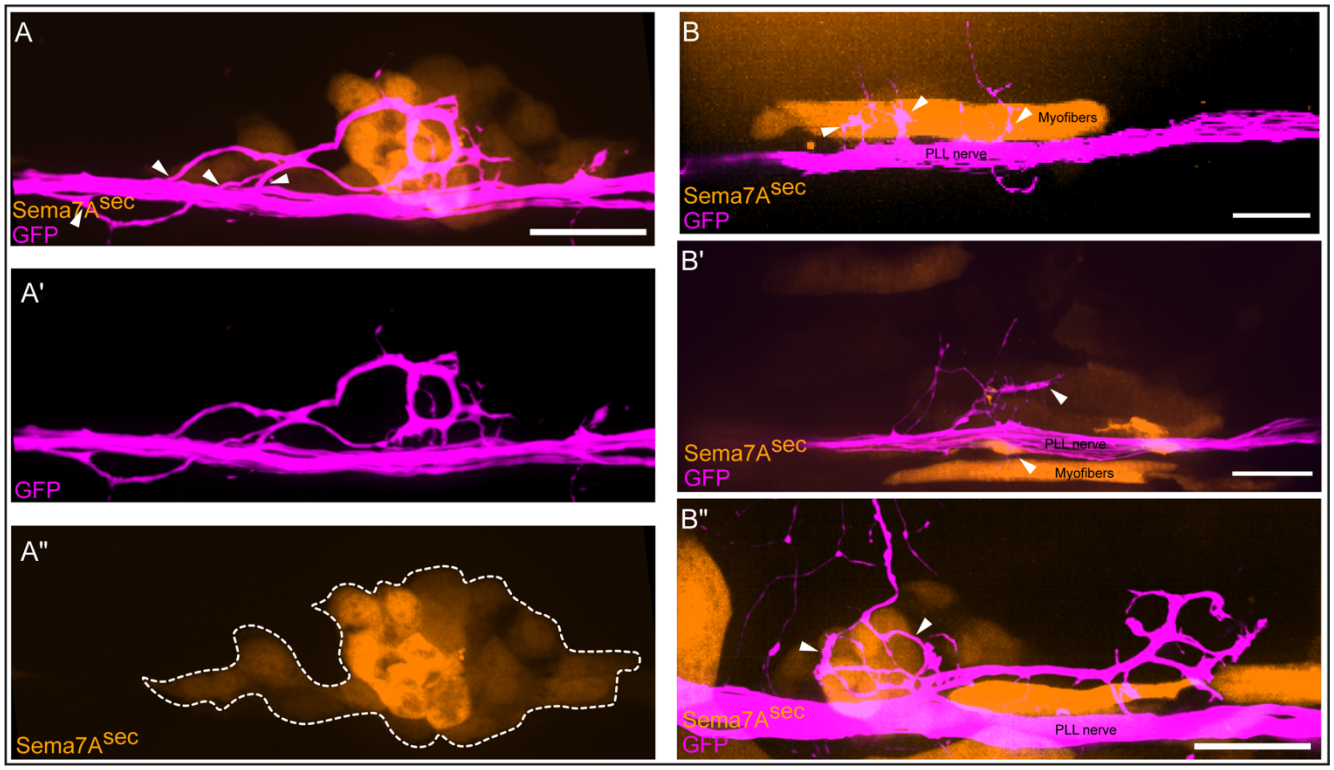

Supplementary Figure 3. Ectopic Sema7A^{sec} diffusive cues induce aberrant neural arborizations. (A-A") In a micrograph of an ectopically expressing Sema7A^{sec} (orange) larva, the sensory arbors (magenta) extend multiple aberrant axonal projections (arrowheads) that reenter the lateral line nerve while following an ectopic Sema7A source. Maximal-intensity projections of the sensory arbors and the ectopically expressing Sema7A cells (white dashed line) are shown in A' and A", respectively. (B-B") Micrographs depict three individual incidents of ectopic *sema7a^{sec}* (orange) integrations that occurred distant from neuromasts. In each case, a set of myofibers expresses the ectopic Sema7A^{sec} protein that induces neurite extensions (arrowheads) from the lateral line nerve (magenta) toward itself. Scale bars, 20 μm.

Supplementary Movie 3. Sensory axonal projections contact an embryonic muscle progenitor cell expressing Sema7A^{sec}. A through-focus scan of a 3 dpf larva depicts a muscle progenitor cell in the dermomyotome that expresses the ectopic Sema7A^{sec} (orange) and the sensory axonal projection (magenta) that makes intimate contact with it.

Supplementary Movie 4. Volumetric surface reconstruction of a sensory arbor and an embryonic muscle progenitor expressing Sema7A^{sec}. Reconstruction of the muscle progenitor cell (orange) at 3 dpf reveals its intimate association with an attracted sensory arbor (magenta).

Supplementary Movie 5. Sensory axonal projections remain in proximity to myofibers expressing Sema7A^{sec}. A through-focus scan of a 3 dpf larva depicts mature myofibers expressing exogenous Sema7A^{sec} deep in the myotome (orange) and the sensory axonal projection (magenta) that remains nearby.

Supplementary Movie 6. Volumetric surface reconstruction of a sensory arbor and the mature myofibers expressing Sema7A^{sec}. Reconstruction of mature myofibers expressing ectopic Sema7A^{sec} (orange) at 3 dpf shows their close association with the attracted sensory arbors (magenta).

Supplementary Movie 7. Aberrant axonal projections reenter the lateral line nerve while following an ectopic Sema7A^{sec} source. A through-focus scan of a 3 dpf larva depicts cells expressing exogenous Sema7A^{sec} (orange) that guides the aberrant sensory axonal projection (magenta) back into the lateral line nerve. Scale bar, 20 μm.

Supplementary Movie 8, 9, and 10. Ectopic Sema7A^{sec} expression induces aberrant neurite projections from the lateral line nerve. Through-focus scans of 3 dpf larvae depict three individual incidents of ectopic *sema7a^{sec}* (orange) integrations that occurred distant from the neuromasts. In each case, myofibers express ectopic Sema7A^{sec} protein that attracts neurite extensions (arrowheads) from the lateral line nerve (magenta). Scale bars, 20 μm.

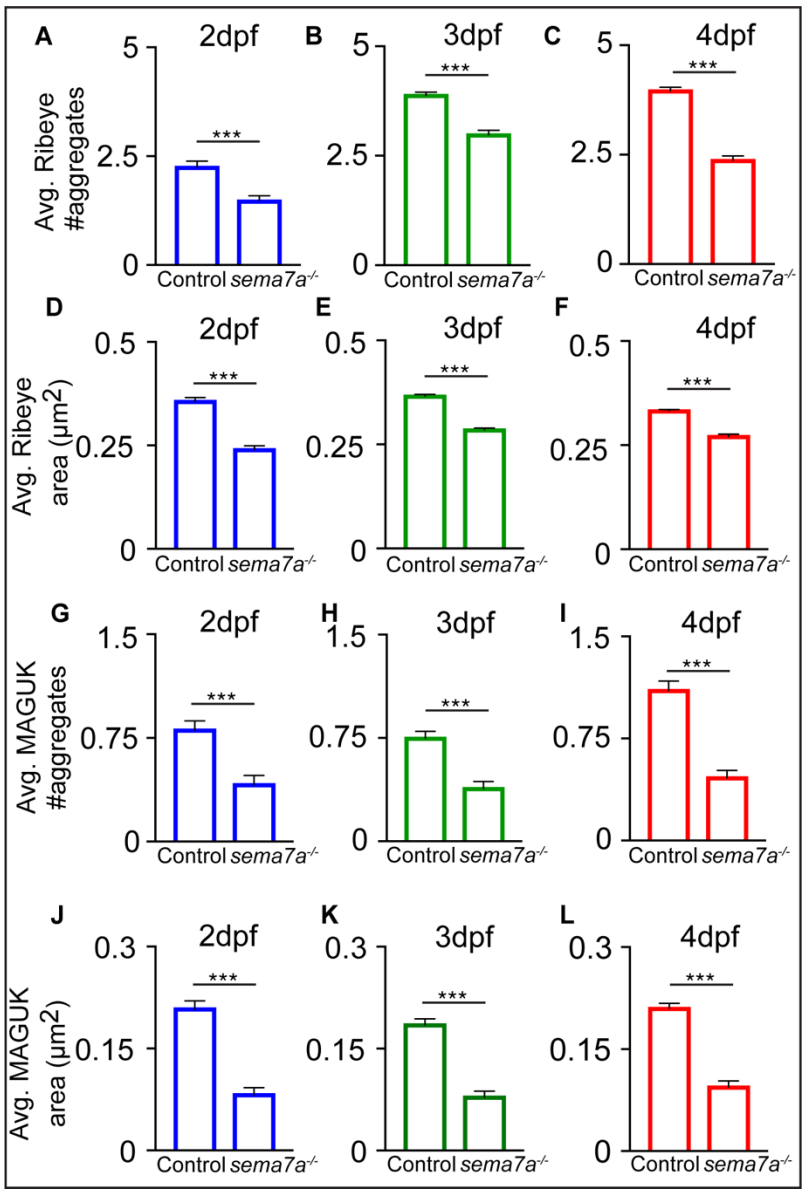

Supplementary Figure 4. *sema7a*$^{-/-}$ mutants display impaired synaptic assembly. (A-F) The plots quantitate the average numbers and areas of presynaptic aggregates from control and *sema7a*$^{-/-}$ neuromasts. Significant decreases in the numbers and areas of presynaptic aggregates are observed across development. Three hundred and forty-one, 1229, and 1286 presynaptic aggregates were analyzed from 2 dpf, 3 dpf, and 4 dpf control larvae, respectively. Two hundred and thirty-five, 643, and 419 presynaptic aggregates were analyzed from 2 dpf, 3 dpf, and 4 dpf *sema7a*$^{-/-}$ mutant larvae, respectively. (G-L) The plots quantitate the average numbers and areas of postsynaptic aggregates from control and *sema7a*$^{-/-}$ neuromasts. Significant decreases in the numbers and areas of postsynaptic aggregates occurred during development. Three hundred and ninety-seven, 1243, and 1300 postsynaptic

aggregates were analyzed from 2 dpf, 3 dpf, and 4 dpf control larvae, respectively. Three hundred and four, 651, and 451 postsynaptic aggregates were analyzed from 2 dpf, 3 dpf, and 4 dpf *sema7a*$^{-/-}$ mutant larvae, respectively. Means ± SEMs; *** implies $p < 0.001$.

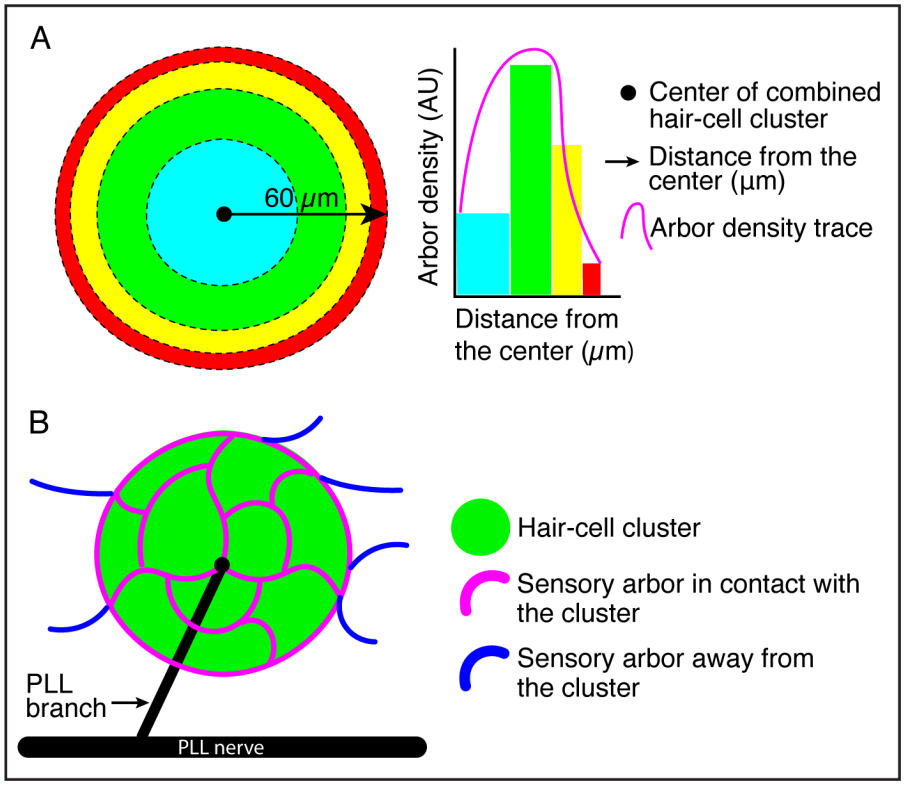

Supplementary Figure 5. Quantification of sensory arbor distributions and contacts with hair cell clusters. (A) A schematic drawing of the combined hair cell cluster and surrounding region depicts concentric sections of equal area in distinct colors (cyan, green, yellow, and blue). The arbor density is plotted as a histogram against the distance (black arrow) from the center (black circle) of the combined hair cell cluster. The histogram is represented as a density trace graph (magenta). (B) A schematic drawing of a posterior lateral line neuromast depicts the posterior lateral line (PLL) nerve (black), posterior lateral line branch (black), the sensory arbors (magenta) that contact the hair cell cluster (green), and the sensory arbors that project away (blue) from the hair cell cluster.

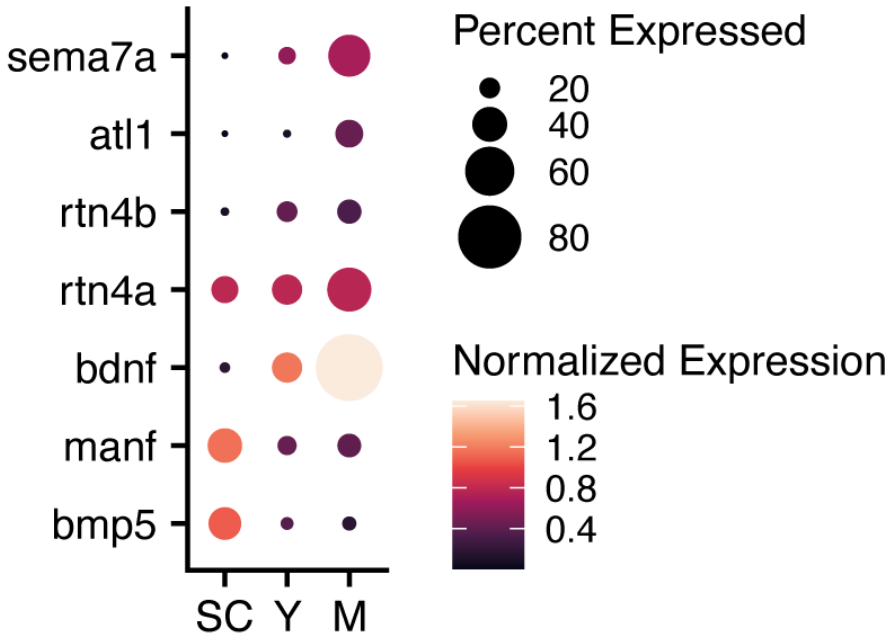

Supplementary Figure 6. Expression of diverse neural guidance cues in developing neuromasts. Analysis of single cell RNA-sequencing data (9) shows the expression of multiple neural guidance genes that are expressed across young hair cells (Y), mature hair cells (M), and support cells (SC). Dot sizes and colors signify the proportion of cells in each cluster that express a gene and the average strength of expression (ln[(counts/10,000) +1]), respectively.

1. Lykissas M, Batistatou A, Charalabopoulos K, Beris A. The Role of Neurotrophins in Axonal Growth, Guidance, and Regeneration. Curr Neurovasc Res. 2007 May 1;4(2):143–51.
2. Vaccaro G, Dumoulin A, Zuñiga NR, Bandtlow CE, Stoeckli ET. The Nogo-66 Receptors NgR1 and NgR3 Are Required for Commissural Axon Pathfinding. J Neurosci. 2022 May 18;42(20):4087–100.
3. Nguyen-Ba-Charvet KT, Di Meglio T, Fouquet C, Chedotal A. Robos and Slits Control the Pathfinding and Targeting of Mouse Olfactory Sensory Axons. J Neurosci. 2008 Apr 16;28(16):4244–9.
4. Jeroen Pasterkamp R, Peschon JJ, Spriggs MK, Kolodkin AL. Semaphorin 7A promotes axon outgrowth through integrins and MAPKs. Nature. 2003 Jul;424(6947):398–405.
5. Nagiel A, Andor-Ardo D, Hudspeth AJ. Specificity of Afferent Synapses onto Plane-Polarized Hair Cells in the Posterior Lateral Line of the Zebrafish. J Neurosci. 2008 Aug 20;28(34):8442–53.
6. Jacobo A, Dasgupta A, Erzberger A, Siletti K, Hudspeth AJ. Notch-Mediated Determination of Hair-Bundle Polarity in Mechanosensory Hair Cells of the Zebrafish Lateral Line. Curr Biol. 2019 Nov;29(21):3579-3587.e7.
7. Valera G, Markov DA, Bijari K, Randlett O, Asgharsharghi A, Baudoin JP, et al. A neuronal blueprint for directional mechanosensation in larval zebrafish. Curr Biol. 2021 Apr;31(7):1463-1475.e6.
8. Dow E, Jacobo A, Hossain S, Siletti K, Hudspeth AJ. Connectomics of the zebrafish's lateral-line neuromast reveals wiring and miswiring in a simple microcircuit. eLife. 2018 Jun 12;7:e33988.
9. Lush ME, Diaz DC, Koenecke N, Baek S, Boldt H, St Peter MK, et al. scRNA-Seq reveals distinct stem cell populations that drive hair cell regeneration after loss of Fgf and Notch signaling. eLife. 2019 Jan 25;8:e44431.
10. Carulli D, de Winter F, Verhaagen J. Semaphorins in Adult Nervous System Plasticity and Disease. Front Synaptic Neurosci. 2021 May 11;13:672891.

692 11. Yazdani U, Terman JR. The semaphorins. Genome Biol. 2006;7(3):211.
693 12. de Winter F, Kwok JCF, Fawcett JW, Vo TT, Carulli D, Verhaagen J. The Chemorepulsive
694 Protein Semaphorin 3A and Perineuronal Net-Mediated Plasticity. Neural Plast.
695 2016;2016:1–14.
696 13. Coate TM, Spita NA, Zhang KD, Isgrig KT, Kelley MW. Neuropilin-2/Semaphorin-3F-
697 mediated repulsion promotes inner hair cell innervation by spiral ganglion neurons. eLife.
698 2015 Aug 24;4:e07830.
699 14. Carcea I, Patil SB, Robison AJ, Mesias R, Huntsman MM, Froemke RC, et al. Maturation
700 of cortical circuits requires Semaphorin 7A. Proc Natl Acad Sci. 2014 Sep
701 23;111(38):13978–83.
702 15. Inoue N, Nishizumi H, Naritsuka H, Kiyonari H, Sakano H. Sema7A/PlxnCl signaling
703 triggers activity-dependent olfactory synapse formation. Nat Commun. 2018
704 Dec;9(1):1842.
705 16. Inoue N, Nishizumi H, Ooyama R, Mogi K, Nishimori K, Kikusui T, et al. The olfactory
706 critical period is determined by activity-dependent Sema7A/PlxnC1 signaling within
707 glomeruli. eLife. 2021 Mar 29;10:e65078.
708 17. Morote-Garcia JC, Napiwotzky D, Köhler D, Rosenberger P. Endothelial Semaphorin 7A
709 promotes neutrophil migration during hypoxia. Proc Natl Acad Sci. 2012 Aug
710 28;109(35):14146–51.
711 18. Nishide M, Kumanogoh A. The role of semaphorins in immune responses and
712 autoimmune rheumatic diseases. Nat Rev Rheumatol. 2018 Jan;14(1):19–31.
713 19. Köhler D, Granja T, Volz J, Koeppen M, Langer HF, Hansmann G, et al. Red blood cell-
714 derived semaphorin 7A promotes thrombo-inflammation in myocardial ischemia-
715 reperfusion injury through platelet GPIb. Nat Commun. 2020 Dec;11(1):1315.
716 20. Pham TL, He J, Kakazu AH, Jun B, Bazan NG, Bazan HEP. Defining a mechanistic link
717 between pigment epithelium–derived factor, docosahexaenoic acid, and corneal nerve
718 regeneration. J Biol Chem. 2017 Nov;292(45):18486–99.
719 21. Xie J, Wang H. Semaphorin 7A as a potential immune regulator and promising

720 therapeutic target in rheumatoid arthritis. Arthritis Res Ther. 2017 Dec;19(1):10.
721 22. Dow E, Siletti K, Hudspeth AJ. Cellular projections from sensory hair cells form polarity-
722 specific scaffolds during synaptogenesis. Genes Dev. 2015 May 15;29(10):1087–94.
723 23. Pujol-Martí J, Faucherre A, Aziz-Bose R, Asgharsharghi A, Colombelli J, Trapani JG, et
724 al. Converging Axons Collectively Initiate and Maintain Synaptic Selectivity in a Constantly
725 Remodeling Sensory Organ. Curr Biol. 2014 Dec;24(24):2968–74.
726 24. De Wit J, De Winter F, Klooster J, Verhaagen J. Semaphorin 3A displays a punctate
727 distribution on the surface of neuronal cells and interacts with proteoglycans in the
728 extracellular matrix. Mol Cell Neurosci. 2005 May;29(1):40–55.
729 25. Sharma P, Ruel TD, Kocha KM, Liao S, Huang P. Single cell dynamics of embryonic
730 muscle progenitor cells in zebrafish. Development. 2019 Jan 1;dev.178400.
731 26. Keenan SR, Currie PD. The Developmental Phases of Zebrafish Myogenesis. J Dev Biol.
732 2019 Jun 2;7(2):12.
733 27. Sato A, Koshida S, Takeda H. Single-cell analysis of somatotopic map formation in the
734 zebrafish lateral line system. Dev Dyn. 2010 Jul;239(7):2058–65.
735 28. Shen K, Cowan CW. Guidance Molecules in Synapse Formation and Plasticity. Cold
736 Spring Harb Perspect Biol. 2010 Apr 1;2(4):a001842–a001842.
737 29. Um JW, Ko J. Neural Glycosylphosphatidylinositol-Anchored Proteins in Synaptic
738 Specification. Trends Cell Biol. 2017 Dec;27(12):931–45.
739 30. Uesaka N, Uchigashima M, Mikuni T, Nakazawa T, Nakao H, Hirai H, et al. Retrograde
740 semaphorin signaling regulates synapse elimination in the developing mouse brain.
741 Science. 2014 May 30;344(6187):1020–3.
742 31. Sheets L, Hagen MW, Nicolson T. Characterization of Ribeye Subunits in Zebrafish Hair
743 Cells Reveals That Exogenous Ribeye B-Domain and CtBP1 Localize to the Basal Ends
744 of Synaptic Ribbons. Riley B, editor. PLoS ONE. 2014 Sep 10;9(9):e107256.
745 32. Oliva C, Escobedo P, Astorga C, Molina C, Sierralta J. Role of the maguk protein family in
746 synapse formation and function. Dev Neurobiol. 2012 Jan;72(1):57–72.
747 33. Suli A, Pujol R, Cunningham DE, Hailey DW, Prendergast A, Rubel EW, et al. Innervation

regulates synaptic ribbons in lateral line mechanosensory hair cells. J Cell Sci. 2016 Jan 1;jcs.182592.

34. Taschenberger H, Leão RM, Rowland KC, Spirou GA, von Gersdorff H. Optimizing Synaptic Architecture and Efficiency for High-Frequency Transmission. Neuron. 2002 Dec;36(6):1127–43.

35. Myers JP, Gomez TM. Focal Adhesion Kinase Promotes Integrin Adhesion Dynamics Necessary for Chemotropic Turning of Nerve Growth Cones. J Neurosci. 2011 Sep 21;31(38):13585–95.

36. O'Donnell M, Chance RK, Bashaw GJ. Axon Growth and Guidance: Receptor Regulation and Signal Transduction. Annu Rev Neurosci. 2009 Jun 1;32(1):383–412.

37. Gilmour D, Knaut H, Maischein HM, Nüsslein-Volhard C. Towing of sensory axons by their migrating target cells in vivo. Nat Neurosci. 2004 May;7(5):491–2.

38. Metcalfe WK. Sensory neuron growth cones comigrate with posterior lateral line primordial cells in zebrafish. J Comp Neurol. 1985 Aug 8;238(2):218–24.

39. Gasanov EV, Rafieva LM, Korzh VP. BDNF-TrkB Axis Regulates Migration of the Lateral Line Primordium and Modulates the Maintenance of Mechanoreceptor Progenitors. Proost P, editor. PLOS ONE. 2015 Mar 9;10(3):e0119711.

40. Schuster K, Dambly-Chaudière C, Ghysen A. Glial cell line-derived neurotrophic factor defines the path of developing and regenerating axons in the lateral line system of zebrafish. Proc Natl Acad Sci. 2010 Nov 9;107(45):19531–6.

41. Germanà A, Laurà R, Montalbano G, Guerrera MC, Amato V, Zichichi R, et al. Expression of Brain-Derived Neurotrophic Factor and TrkB in the Lateral Line System of Zebrafish During Development. Cell Mol Neurobiol. 2010 Jul;30(5):787–93.

42. Ji YR, Warrier S, Jiang T, Wu DK, Kindt KS. Directional selectivity of afferent neurons in zebrafish neuromasts is regulated by Emx2 in presynaptic hair cells. eLife. 2018 Apr 19;7:e35796.

43. Kindt KS, Finch G, Nicolson T. Kinocilia Mediate Mechanosensitivity in Developing Zebrafish Hair Cells. Dev Cell. 2012 Aug;23(2):329–41.

776 44. Obholzer N, Wolfson S, Trapani JG, Mo W, Nechiporuk A, Busch-Nentwich E, et al.
777 Vesicular Glutamate Transporter 3 Is Required for Synaptic Transmission in Zebrafish
778 Hair Cells. J Neurosci. 2008 Feb 27;28(9):2110–8.
779 45. Kwan KM, Fujimoto E, Grabher C, Mangum BD, Hardy ME, Campbell DS, et al. The
780 Tol2kit: A multisite gateway-based construction kit forTol2 transposon transgenesis
781 constructs. Dev Dyn. 2007 Nov;236(11):3088–99.
782 46. Arshadi C, Günther U, Eddison M, Harrington KIS, Ferreira TA. SNT: a unifying toolbox
783 for quantification of neuronal anatomy. Nat Methods. 2021 Apr;18(4):374–7.